

Systematic Study of Earthquake Source Mechanism and Regional Stress Field in the Southern Montney Unconventional Play of Northeastern British Columbia (NTS 093P/09, 10, 15, 16, 094A/01, 02, 07, 08)

A. Babaie Mahani, Geoscience BC, Vancouver, British Columbia, ali.mahani@mahangeo.com

Babaie Mahani, A. (2020): Systematic study of earthquake source mechanism and regional stress field in the southern Montney unconventional play of northeastern British Columbia (NTS 093P/09, 10, 15, 16, 094A/01, 02, 07, 08); *in* Geoscience BC Summary of Activities 2019: Energy and Water, Geoscience BC, Report 2020-02, p. 13–18.

Introduction

The Western Canada Sedimentary Basin (WCSB) has experienced a significant increase in both the number and magnitude of earthquakes in the past decade due to fluid injection associated with hydraulic fracturing operations (Schultz et al., 2014; Rubinstein and Babaie Mahani, 2015; Atkinson et al., 2016; Bao and Eaton, 2016; Babaie Mahani et al., 2017; Kao et al., 2018). As a result, continuous improvements in earthquake detection have been made within the unconventional resources of the Montney and Duvernay formations, in northeastern British Columbia (BC) and western Alberta, through densification of seismographic networks (Salas et al., 2013; Salas and Walker, 2014; Schultz et al., 2015; Babaie Mahani et al., 2016). The addition of new seismographic stations, at close distances from injection sites, have provided the required data for detailed analysis of seismic activity, especially with regard to small-magnitude earthquakes (as low as 1.5) for which sufficient data had not been available.

The source mechanisms of induced earthquakes in the WCSB have been analyzed by several researchers using moment tensor inversion and P-wave first motions (Eaton and Babaie Mahani, 2015; Wang et al., 2016, 2017, 2018; Zhang et al., 2016). Overall, focal mechanisms show a combination of strike-slip and reverse faulting for the events occurring within the Montney and Duvernay formations and along the Rocky Mountain fold and thrust belt (RMFTB) in northeastern BC and western Alberta (Ristau et al., 2007; Babaie Mahani et al., 2017; Kao et al., 2018; Zhang et al., 2019).

In this study, data from local and regional seismographic stations were used to obtain focal mechanisms and parameters of the stress field for 66 earthquakes, which occurred between April 2018 and May 2019, in the southern Montney unconventional play of northeastern BC. These events occurred in an area to the south of Fort St. John and north of

Dawson Creek, where multistage hydraulic fracturing operations have been conducted for several years (Figure 1; Babaie Mahani et al., 2016; Babaie Mahani and Kao, 2018). Residents in the area have felt events with small magnitudes (M) ranging from 1 to 2. Moreover, large peak ground accelerations (PGA) have been recorded at close hypocentral distances (<5 km) from events as small as M 3 (e.g., PGA of >0.1 g with 1 g = 9.8 m/s²; Atkinson and Assatourians, 2017; Babaie Mahani and Kao, 2018).

Tectonic Setting

The main tectonic structure in the study area is the Fort St. John graben (FSJG), which is the predominant graben in the Dawson Creek graben complex. The FSJG was formed during the Carboniferous–Permian period by localized subsidence of the Peace River arch. The Golata, Kiskatinaw and Taylor Flat formations, of the Stoddart Group, successively infilled FSJG, all of them overlying the Debolt Formation. This succession was later overlain with the Permian Belloy and Triassic Montney, Doig, Halfway, Charlie Lake and Baldonnel formations (O’Connell, 1994; Petrel Robertson Consulting Inc., 2015).

Although grabens are associated with normal faulting, the subsidence of the Peace River arch and the formation of FSJG were coupled with strike-slip motion and related compressional and rotational movement during the graben’s development (Barclay et al., 1990). The complex tectonic history of FSJG, including the Laramide orogenic phase, resulted in development of normal, strike-slip and reverse faults, which influenced the Carboniferous Debolt to the Triassic Doig formations (Berger et al., 2009; Dixon, 2011; Petrel Robertson Consulting Inc., 2015; Davies et al., 2018).

Dataset

Due to the increase in seismicity rate and occurrence of several felt events, the BC Oil and Gas Commission (BCOGC) implemented requirements for ground-motion monitoring based on PGA. The initial PGA reporting threshold of 0.02 g introduced in June 2016 was refined to 0.008 g in January 2018. In May 2018, BCOGC instituted the Kiskati-

This publication is also available, free of charge, as colour digital files in Adobe Acrobat® PDF format from the Geoscience BC website: <http://www.geosciencebc.com/updates/summary-of-activities/>.

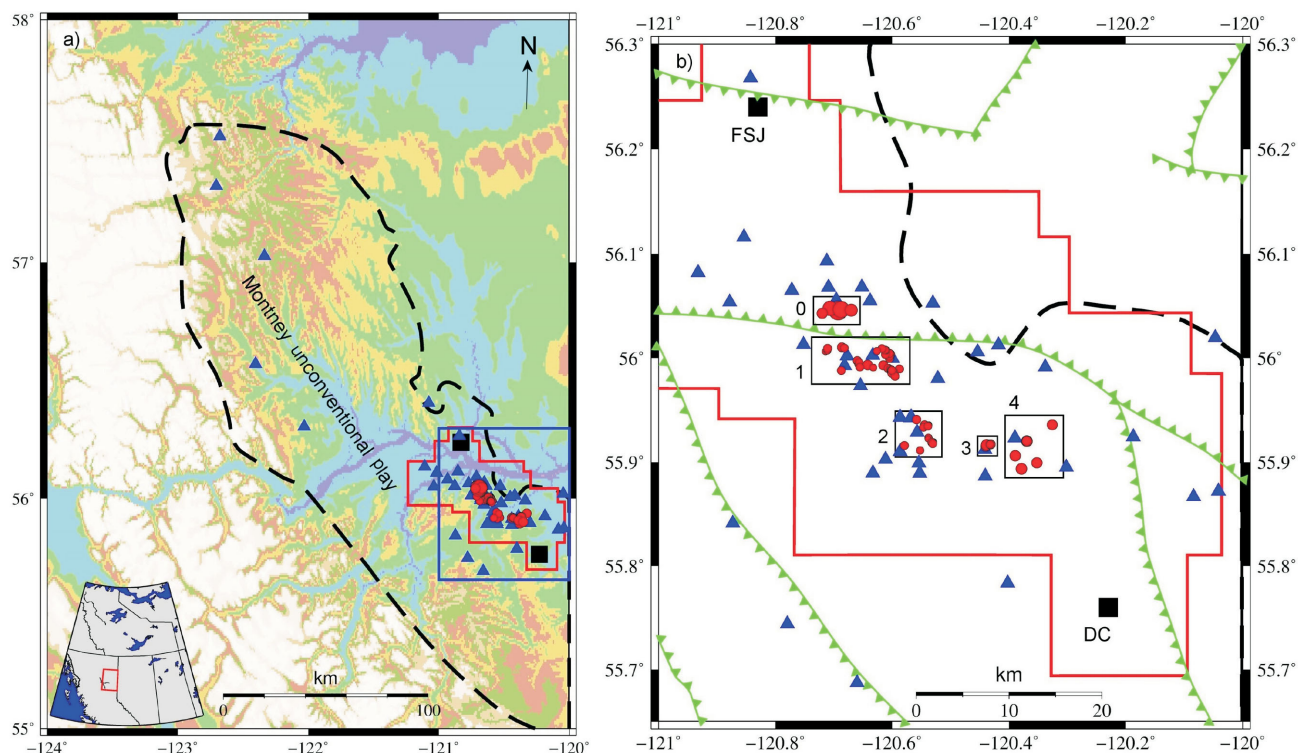


Figure 1. a) The Montney unconventional play (outlined with black dashed line) in northeastern British Columbia. Background image from Linquist et al. (2004) shows the topography. The study area is outlined with a solid blue line. The red line shows the outline of the Kiskatinaw Seismic Monitoring and Mitigation Area. Black solid squares indicate the major cities (FSJ, Fort St. John; DC, Dawson Creek). Earthquakes and seismographic stations are shown with circles and triangles, respectively. Inset map shows the geographic location of the study area with respect to western Canada. **b)** Study area with the areas of the five clusters outlined with solid black lines. Solid green lines show the normal faults associated with the Dawson Creek graben complex (from Davies et al., 2018). Triangles on fault lines depict the hanging wall.

naw Seismic Monitoring and Mitigation Area (KSMMA; Figure 1). Permit holders operating within KSMMA must report to BCOGC any felt event or ground motion equal to or above the assigned threshold in the form of a catalogue containing event parameters such as location, magnitude and ground motion values. Moreover, waveforms from seismographic stations that recorded the higher-than-threshold PGA must be submitted to BCOGC, which are made available to the public via BCOGC’s eLibrary. Most of the events analyzed in this study are small in magnitude ($M < 2$), therefore were only clearly recorded by local seismographic stations within 20 to 30 km of the epicentres. The largest event is the November 30, 2018, hydraulic fracturing–induced earthquake with moment magnitude of 4.6.

Although focal depths reported in earthquake catalogues are usually associated with large uncertainties, induced events within KSMMA mostly have depths in the range of 3 to 4 km, located within the lower Montney, Belloy and Debolt formations (Babaie Mahani and Kao, 2018). Figure 1 shows the distribution of 66 events for which focal mechanisms were obtained and the location of seismographic stations used in this study. These events were grouped into five clusters (0 to 4) based on the proximity of their locations.

Focal Mechanisms

In this study, focal mechanisms were obtained from the P-wave first motions using the vertical components of waveforms that were filtered by a 4th order Butterworth band-pass filter with corner frequencies of 1 and 3 Hz. The 1 Hz high-pass corner frequency was chosen to eliminate prominent long-period trends observed on the majority of seismograms, whereas the 3 Hz low-pass corner frequency was selected to obtain relatively simple waveforms suitable for phase picking. For the purpose of this study, the velocity model and the methodology described by Eaton and Babaie Mahani (2015) were followed to determine focal mechanisms. Near the surface, the velocity model incorporates two sedimentary layers totalling 4.5 km in thickness underlain by a 35 km thick crystalized basement. The crystalized basement is characterized by a linear velocity gradient with $V_0 = 6$ km/sec and gradient $k = 0.0229$ sec⁻¹. Takeoff angles were determined using this velocity model and ray-tracing results (Eaton and Babaie Mahani, 2015). For all of the solutions obtained here, a source depth of 5 km was assumed, which is situated 500 m below the base of the sedimentary basin. Although, based on the information provided from some hydraulic fracturing wells, depth to the basement can be less than 4.5 km in this area. Figure 2 shows that the

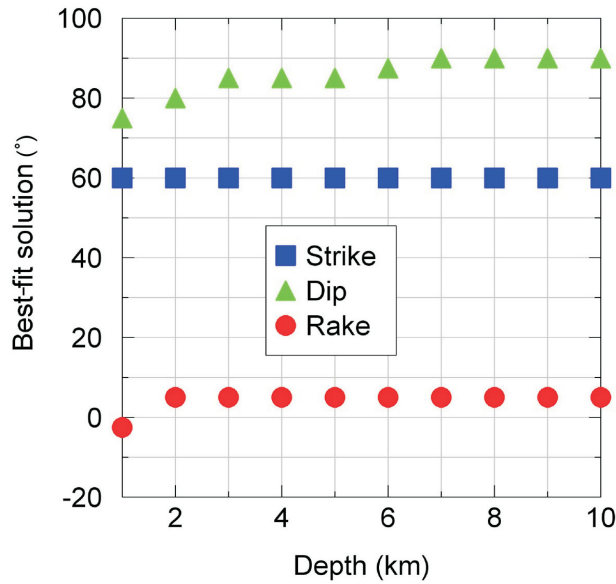


Figure 2. The effect of different depth assumptions on the results of the best-fit solution of focal mechanisms.

solutions are relatively insensitive to focal depth within a focal depth range of 2 to 10 km.

To ensure the reliability of focal mechanisms, only events with at least 10 P-wave polarities were considered. Following this criterion, focal mechanisms for 66 earthquakes were obtained. For each event, the parameters of the best fitting plane were calculated from the average and standard

deviation of strike, dip and rake values of the trial focal mechanisms with the minimum associated error (Eaton and Bahaie Mahani, 2015).

Overall, fault plane solutions show that the prevailing mechanism in all clusters (Figure 1b) is strike-slip with strike of the best fitting plane mostly $\sim 60^\circ$ in clusters 0, 1 and 2. For clusters 3 and 4, however, there is a wider range of strike directions. Moreover, dip angles of the best fitting plane are $>20^\circ$ with most planes having dip angles $>60^\circ$. As an example, Figure 3 shows the focal mechanisms in cluster 1, which includes more earthquakes than the other clusters. In Figure 4, the compression (P) and extension (T) axes are shown for the focal mechanisms in each cluster based on the best fitting nodal plane. Although there is scatter in data points, the P and T axes mostly have low plunges with the trends of northeast-southwest and northwest-southeast, respectively. Similar results were obtained using the auxiliary nodal plane. The trends of the P and T axes are consistent with other studies for earthquakes in the WCSB and along the RMFTB (Ristau et al., 2007).

Stress Tensor Inversion

Focal mechanisms determined from the P-wave first motions or moment tensor inversion can be used to invert the stress tensor of a regional stress field (Michael, 1987). An important factor in stress inversion is to decide which nodal plane is the actual causative fault. Aftershock distribution or robust constraint on earthquake locations are usually

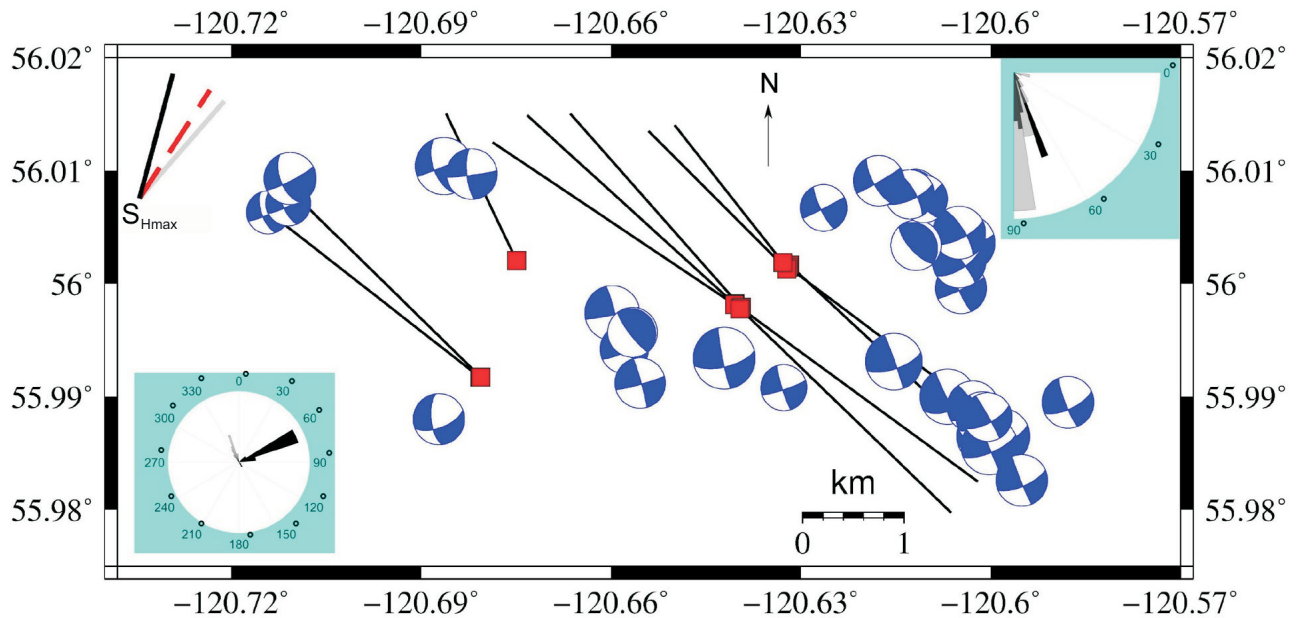


Figure 3. Focal mechanisms derived from P-wave first motions for events in cluster 1 (Figure 1b). The three lines in the upper left corner show the orientation of maximum horizontal stress from the World Stress Map (grey solid line; Heidbach et al., 2016) and from stress inversion results of this study using the best fitting (red dashed line) and auxiliary (solid black line) planes. Polar diagrams show the dip and strike distributions for the best fitting (black) and auxiliary (grey) nodal planes. Dark grey shows overlapping values. Squares show the location of the hydraulic fracturing wells in the area with black solid lines showing the surface projection of the horizontal extent of these wells.

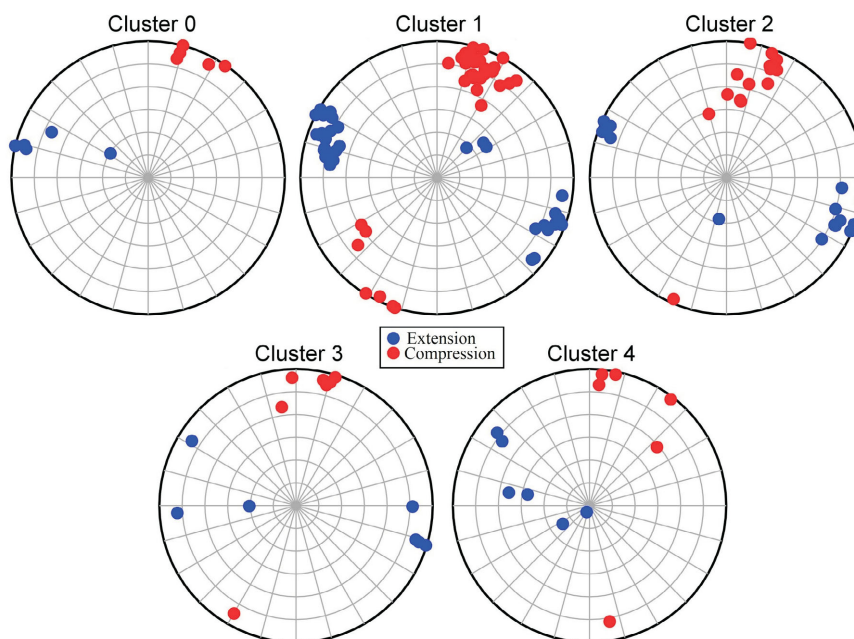


Figure 4. Orientation of the compression (P) and extension (T) axes for all the events in each cluster (Figure 1b). Results are shown for the best fitting nodal plane of the focal mechanisms.

good sources of information for this purpose. In this study, however, most events are small and there are statistically not enough events to unambiguously identify the fault orientation in each cluster. Here, the stress inversion is applied for both nodal planes and the results are compared with values from the World Stress Map (WSM; Heidbach et al., 2016).

Usually four parameters are calculated for the stress field using focal mechanisms; the orientation of three principal compressive stresses ($S_1 > S_2 > S_3$) and a relative measure of the magnitude of the intermediate principal stress (R; Etchecopar et al., 1981; Gephart and Forsyth, 1984; Lund and Townend, 2007) as

$$R = (S_1 - S_2) / (S_1 - S_3) \quad (1)$$

The relative stress magnitude (R) quantifies whether the magnitude of the intermediate (S_2) principal stress is closer to the magnitude of the most (S_1) compressive principal stress or the least (S_3) compressive principal stress. Whereas small values of R imply that S_1 and S_2 are close in magnitude, large values of R imply that S_1 and S_3 have similar magnitudes.

Martinez-Garzon et al. (2014) provided a MATLAB package for stress inversion from earthquake focal mechanisms. Their inversion provides the orientation of S_1 , S_2 and S_3 and R, thus suitable for the purpose of this study. Using the focal mechanism parameters (dip direction, dip and rake) in each cluster, stress inversion was applied in each cluster. Table 1 shows the trend and plunge of the best solutions for the three principal stresses and R in each cluster using both

Table 1. Results of stress inversion for each cluster based on the Martinez-Garzon et al. (2014) inversion module using both the best fitting (in bold) and the auxiliary nodal planes of focal mechanisms. The three principal compressive stresses are S_1 , S_2 and S_3 and the relative stress magnitude is R. The trend of maximum horizontal stress (S_{Hmax}) is based on the relationships provided in Lund and Townend (2007). Trends are clockwise from north.

Cluster ID	Trend S_1 (°)	Plunge S_1 (°)	Trend S_2 (°)	Plunge S_2 (°)	Trend S_3 (°)	Plunge S_3 (°)	R	S_{Hmax} (°)
0	33	3	310	68	122	22	0.8	32
1	34	2	307	56	122	33	0.8	33
2	26	3	290	63	118	27	0.6	30
3	21	1	289	56	112	34	0.8	22
4	22	2	290	40	115	50	0.9	22
0	21	7	179	82	291	3	0.8	18
1	19	7	186	83	289	2	0.6	15
2	13	13	181	77	283	3	0.6	10
3	14	9	179	81	284	2	0.7	11
4	15	12	141	69	282	16	0.6	5

the best fitting and auxiliary nodal planes of focal mechanisms.

The best solution for S_1 has an average plunge of 2° and an average trend of 27° over all clusters using the best fitting nodal planes. On the other hand, average values of 10° and 17° were obtained for the plunge and trend of S_1 for the auxiliary nodal planes. The plunge of the best solution for S_3 is quite different between using the best fitting and the auxiliary planes of focal mechanisms. S_3 increases from 22° to 50° from cluster 0 to 4 with an average trend of 118° over all clusters when using the best fitting nodal plane. On the other hand, S_3 remains fairly horizontal for clusters 0, 1, 2 and 3 and increases to 16° in cluster 4 with an average trend of 286° using the auxiliary plane. As expected, the plunge of S_2 follows the opposite direction to S_3 and decreases from cluster 0 to 4 but remains closer to vertical for the case when the auxiliary plane was used in the stress tensor inversion.

Although, prior to stress inversion, the actual causative fault was not clear, the results from stress inversion are consistent between the best fitting and auxiliary nodal planes suggesting a major strike-slip component and a minor reverse mechanism for the earthquakes in this area. This can also be observed from the relative stress magnitude (R) in Table 1, suggesting a strike-slip/reverse faulting regime. Since S_1 and S_3 are not perfectly horizontal and S_2 is not vertical, the trend of S_1 is not exactly the same as the maximum horizontal stress (S_{Hmax}). In Table 1, the trend of S_{Hmax} is shown using the relationships provided by Lund and Townend (2007). In Figure 3, the trend of S_{Hmax} is plotted and compared with the value from WSM, which is from two borehole breakout measurements in the study area. The trend of S_{Hmax} from the best fitting nodal plane is close to the average trend value of 41° from WSM (Heidbach et al., 2016). The trend in the study area varies from 22° to 33° for the best fitting nodal plane and varies from 5° to 18° for the auxiliary nodal plane.

Conclusion

Focal mechanisms for several induced earthquakes caused by hydraulic fracturing within the Montney unconventional play of northeastern British Columbia were determined for this study. Using the polarities of the first P-wave motion, focal mechanisms for 66 events, for which there were at least 10 recordings each, were obtained. Magnitudes of these events were between 1.5 and 4.6 and were distributed in five clusters based on the proximity of epicentres. Results show that strike-slip movement is the prevailing source mechanism for the events in this area, although reverse faulting was also observed for a few earthquakes. The best fitting nodal plane mostly strikes at $\sim 60^\circ$ with most events having dip angles of $>60^\circ$. For each cluster, the orientation of the three principal compressive

stresses ($S_1 > S_2 > S_3$) and the relative intermediate principal stress magnitude (R) were calculated. Assuming the best fitting nodal plane to be the causative fault, the plunge of S_1 varies between 1° to 3° with its trend varying between 21° to 34° across the clusters. On the other hand, the plunge of S_3 varies between 22° and 50° with its trend varying between 112° and 122° . The relative stress magnitude shows values between 0.6 and 0.9 suggesting that the magnitude of the intermediate (S_2) and the least compressive stress (S_3) are similar, which is consistent with a strike-slip/reverse faulting regime. The trend of maximum horizontal stress (S_{Hmax}) was estimated from the four parameters (S_1, S_2, S_3, R) obtained during stress inversion. The trend of S_{Hmax} varies from 22° to 33° , using the best fitting nodal plane, which is slightly lower than the average trend of S_{Hmax} from the World Stress Map (41°).

Acknowledgments

The author thanks A. Gamp for his constructive comments on this manuscript. The author also appreciates P. Martinez-Garzon for her consultation on stress inversion. The Seismological Research Letters' editor in chief, A. Bent, and two anonymous reviewers are thanked for their thorough review of this paper. This work was partially supported by the BC Seismic Research Consortium (Geoscience BC, BC Oil and Gas Research and Innovation Society, Canadian Association of Petroleum Producers, BC Oil and Gas Commission and Yukon Geological Survey), the Natural Sciences and Engineering Research Council of Canada, and the Environmental Geoscience Program of Natural Resources Canada.

References

- Atkinson, G.M. and Assatourians, K. (2017): Are ground-motion models derived from natural events applicable to the estimation of expected motions for induced earthquakes?; *Seismological Research Letters*, v. 88, p. 430–441.
- Atkinson, G.M., Eaton, D., Ghofrani, H., Walker, D., Cheadle, B., Schultz, R., Scherbakov, R., Tiampo, K., Gu, Y.J., Harrington, R.M., Liu, Y., van der Baan, M. and Kao, H. (2016): Hydraulic fracturing and seismicity in the Western Canada Sedimentary Basin; *Seismological Research Letters*, v. 87, p. 631–647.
- Babaie Mahani, A. and Kao, H. (2018): Ground motion from M 1.5 to 3.8 induced earthquakes at hypocentral distance <45 km in the Montney play of northeast British Columbia, Canada; *Seismological Research Letters*, v. 89, p. 22–34.
- Babaie Mahani, A., Kao, H., Walker, D., Johnson, J. and Salas, C. (2016): Performance evaluation of the regional seismograph network in northeast British Columbia, Canada, for monitoring of induced seismicity; *Seismological Research Letters*, v. 87, p. 648–660.
- Babaie Mahani, A., Schultz, R., Kao, H., Walker, D., Johnson, J. and Salas, C. (2017): Fluid injection and seismic activity in the northern Montney play, British Columbia, Canada, with special reference to the 17 August 2015 Mw 4.6 induced

- earthquake; *Bulletin of Seismological Society of America*, v. 107, p. 542–552.
- Bao, X. and Eaton, D.W. (2016): Fault activation by hydraulic fracturing in western Canada; *Science*, v. 354, p. 1406–1409.
- Barclay, J.E., Krause, F.F., Campbell, R.I. and Utting, J. (1990): Dynamic casting and growth faulting: Dawson Creek Graben Complex, Carboniferous-Permian Peace River Embayment, western Canada; *Bulletin of Canadian Petroleum Geology*, v. 38A, p. 115–145.
- Berger, Z., Beast, M. and Mushayandebvu, M. (2009): The contribution of integrated HRAM studies to exploration and exploitation of unconventional plays in North America, part 2: basement structures control on the development of the Peace River Arch's Montney/Doig resource plays; *The Reservoir*, v. 36, p. 40–45.
- Davies, G., Watson, N., Moslow, T. and MacEachern, J. (2018): Regional subdivisions, sequences, correlations, and facies relationships of the Lower Triassic Montney Formation, west-central Alberta to northeastern British Columbia, Canada, with emphasis on role of paleostructure; *Bulletin of Canadian Petroleum Geology*, v. 66, p. 23–92.
- Dixon, J. (2011): A review of the character and interpreted origins of thick, mudstone-encased sandstone bodies in the Middle Triassic Doig Formation of western Canada; *Bulletin of Canadian Petroleum Geology*, v. 59, p. 261–276.
- Eaton, D.W. and Babaie Mahani, A. (2015): Focal mechanisms of some inferred induced earthquakes in Alberta, Canada; *Seismological Research Letters*, v. 86, p. 1078–1085.
- Etchecopar, A., Vasseur, G. and Daignieres, M. (1981): An inverse problem in microtectonics for the determination of stress tensors from fault striation analysis; *Journal of Structural Geology*, v. 3, p. 51–65.
- Gephart, J.W. and Forsyth, D.W. (1984): An improved method for determining the regional stress tensor using earthquake focal mechanism data: application to the San Fernando earthquake sequence; *Journal of Geophysical Research*, v. 89, p. 9305–9320.
- Heidbach, O., Rajabi, M., Reiter, K., Ziegler, M. and WSM Team (2016): World Stress Map, database release 2016, ver. 1.1; GFZ Data Services, URL <<https://doi.org/10.5880/WSM.2016.001>> [October 2019].
- Kao, H., Hyndman, R.D., Jiang, Y., Visser, R., Smith, B., Babaie Mahani, A., Leonard, L., Ghofrani, H. and He, J. (2018): Induced seismicity in western Canada linked to tectonic strain rate: implications for regional seismic hazard; *Geophysical Research Letters*, v. 45, p. 11 104–11 115.
- Lindquist, K.G., Engle, K., Stahlke, D. and Price, E. (2004): Global topography and bathymetry grid improves research efforts; *Eos, Transactions, American Geophysical Union*, v. 85, no. 19, p. 186, URL <<http://onlinelibrary.wiley.com/doi/10.1029/2004EO190003/full>> [November 2019].
- Lund, B. and Townend, J. (2007): Calculating horizontal stress orientations with full or partial knowledge of the tectonic stress tensor; *Geophysical Journal International*, v. 170, p. 1328–1335.
- Martinez-Garzon, P., Kwiatek, G., Ickrath, M. and Bohnhoff, M. (2014): MSATSI: a MATLAB package for stress inversion combining solid classic methodology, a new simplified user-handling, and a visualization tool; *Seismological Research Letters*, v. 85, p. 896–904.
- Michael, A.J. (1987): Use of focal mechanisms to determine stress: a control study; *Journal of Geophysical Research*, v. 92, p. 357–368.
- O'Connell, S.C. (1994): Geological history of the Peace River Arch; *in Geological Atlas of the Western Canada Sedimentary Basin*, G.D. Mossop and I. Shetsen (comp.), Canadian Society of Petroleum Geologists, Calgary, Alberta, and Alberta Research Council, Edmonton, Alberta, p. 431–438, URL <<https://ags.aer.ca/reports/atlas-of-the-western-canada-sedimentary-basin.htm>> [October 2019].
- Petrel Robertson Consulting Inc. (2015): Characterization of Belloy and Debolt water disposal zones in the Montney play fairway, northeast B.C.; Geoscience BC, Report 2015-03, 45 p., URL <<http://www.geosciencebc.com/reports/gbcr-2015-03/>> [October 2019].
- Ristau, J., Rogers, G.C. and Cassidy, J.F. (2007): Stress in western Canada from regional moment tensor analysis; *Canadian Journal of Earth Sciences*, v. 44, p. 127–148.
- Rubinstein, J.L. and Babaie Mahani, A. (2015): Myths and facts on wastewater injection, hydraulic fracturing, enhanced oil recovery, and induced seismicity; *Seismological Research Letters*, v. 86, p. 1060–1067.
- Salas, C.J. and Walker, D. (2014): Update on regional seismograph network in northeastern British Columbia (NTS 094C, G, I, O, P); *in Geoscience BC Summary of Activities 2013*, Geoscience BC, Report 2014-01, p. 123–126, URL <http://cdn.geosciencebc.com/pdf/SummaryofActivities2013/SoA2013_SalasWalker.pdf> [October 2019].
- Salas, C.J., Walker, D. and Kao, H. (2013): Creating a regional seismograph network in northeastern British Columbia to study the effect of induced seismicity from unconventional gas completions (NTS 094C, G, I, O, P); *in Geoscience BC Summary of Activities 2012*, Geoscience BC, Report 2013-01, p. 131–134, URL <http://cdn.geosciencebc.com/pdf/SummaryofActivities2012/SoA2012_Salas_Seismograph_Network.pdf> [October 2019].
- Schultz, R., Stern, V. and Gu, Y.J. (2014): An investigation of seismicity clustered near the Cordell Field, west central Alberta, and its relation to a nearby disposal well; *Journal of Geophysical Research*, v. 119, p. 3410–3423.
- Schultz, R., Stern, V., Gu, Y.J. and Eaton, D. (2015): Detection threshold and location resolution of the Alberta Geological Survey earthquake catalogue; *Seismological Research Letters*, v. 86, p. 385–397.
- Wang, R., Gu, Y.J., Schultz, R. and Chen, Y. (2018): Faults and non-double-couple components for induced earthquakes; *Geophysical Research Letters*, v. 45, p. 8966–8975.
- Wang, R., Gu, Y.J., Schultz, R., Kim, A. and Atkinson, G. (2016): Source analysis of a potential hydraulic-fracturing-induced earthquake near Fox Creek, Alberta; *Geophysical Research Letters*, v. 43, p. 564–573.
- Wang, R., Gu, Y.J., Schultz, R., Zhang, M. and Kim, A. (2017): Source characteristics and geological implications of the January 2016 induced earthquake swarm near Crooked Lake, Alberta; *Geophysical Journal International*, v. 210, p. 979–988.
- Zhang, H., Eaton, D.W., Li, G., Liu, Y. and Harrington, R.M. (2016): Discriminating induced seismicity from natural earthquakes using moment tensors and source spectra; *Journal of Geophysical Research*, v. 121, p. 972–993.
- Zhang, H., Eaton, D.W., Rodriguez, G. and Jia, S.Q. (2019): Source mechanism analysis and stress inversion for hydraulic-fracturing-induced event sequences near Fox Creek, Alberta; *Bulletin of Seismological Society of America*, v. 109, p. 636–651.